2019-01-01

Dynamic Triggering Of Earthquakes Within The State Of Utah, Usa

David Lewis Guenaga
University of Texas at El Paso, davidguenaga@gmail.com

DYNAMIC TRIGGERING OF EARTHQUAKES WITHIN THE STATE OF UTAH, USA

DAVID L. GUENAGA

Master's Program in Geophysics

APPROVED:

Aaron A. Velasco, Ph.D., Chair

Marianne Karplus, Ph.D.

Vladik Kreinovich, Ph.D.

Charles Ambler, Ph.D.
Dean of the Graduate School

DYNAMIC TRIGGERING OF EARTHQUAKES WITHIN THE STATE OF UTAH, USA

by

DAVID L. GUENAGA, B.S.

THESIS

Presented to the Faculty of the Graduate School of

The University of Texas at El Paso

in Partial Fulfillment

of the Requirements

for the Degree of

MASTER OF SCIENCE

Department of Geological Sciences

THE UNIVERSITY OF TEXAS AT EL PASO

May 2019

Abstract

Understanding the stress state of faults and the stress needed to trigger earthquakes remains a fundamental goal for understanding the earthquake cycle. We focus on deciphering the stress of faults by studying seismic waves from large, distant earthquakes that trigger local seismicity, called remote or dynamic triggering. Utilizing 17 years of waveform and catalog data (2000-2017) from seismic regional networks (i.e., EarthScope USArray Transportable Array, United States Geological Survey, and University of Utah Regional networks), we search for triggered seismicity in the state of Utah following 227 large magnitude ($M \geq 7$) distant earthquakes. Utah provides a long-standing regional network that has a low magnitude threshold that allows for the analysis of small, triggered events. We apply three distinct approaches: 1) a catalog analysis with a statistical approach, 2) an automatic detection analysis using similar statistics, and 3) a visual inspection of events. Using the UUSS seismic catalog, we identify increased seismicity rates after the passage the transient seismic waves for only 5 large magnitude earthquakes that show potential remote triggering in Utah. For our automated detection analysis, we apply a short term to long term detector to high-pass (5 Hz) across filtered ± 5 hours of waveform data after the origin time of each event for 101 seismic stations to identify potentially remotely triggered earthquakes. We build upon previously developed automated methods and find that 89 $M \geq 7$ earthquakes show potential for triggered seismicity. During the visual inspection, we identify previous uncatalogued small, local earthquakes associated with 65 mainshock earthquakes. Of these 65 mainshock earthquakes, 18 display an increase in seismicity indicative of dynamic triggering. Comparing our three analyses, we find our modified automated method is suitable for highlighting areas prone to dynamic triggering. A comparison of the catalog and visually detection analysis revealed that a majority of the local events (including triggered) are absent from the catalog data. We hypothesize

that this discrepancy is due to these local events having lower magnitudes than those included in the catalog. We also find that most surface waves approach the regional faults perpendicular to strike. We hypothesize that due to the strain experienced during the passage of the surface waves the faults experience an instance of decoupling.

Table of Contents

List of Tables

List of Figures

Introduction

Although earthquakes have been studied extensively for the past century, we still have a relatively limited understanding of the failure mechanisms that control faulting. To address key questions on earthquake generation and mitigation, it remains crucial that we understand the nature of stress that results in fault failure. Faults near failure can be triggered (i.e., generate an earthquake) from 1) tectonic motion, 2) changes in static stress caused by a nearby earthquake, 3) dynamic stress from seismic waves following large earthquakes, and 4) anthropogenic activity, such as injection of fluids that change the normal stress state of faults. Tectonic motion on the order of ~10-50 cm/yr will result in the storage of stress along plate boundaries, until the strength of the rock is exceeded (shear stress equals normal stress, termed Coulomb Failure) creating a sudden motion (an earthquake). Static triggering occurs from permanent changes in the Coulomb stress as a consequence of a larger earthquake; this form of triggering occurs within a few fault lengths (i.e., near-field) from the mainshock (King, Stein, and Lin 1994). Dynamic triggering occurs by the passage of surface waves that cause local transient stress changes that can lead to fault failure (Freed 2005). Induced triggering transpires from anthropogenic activities, such as mining and fluid injection; such processes can lead to a decrease in normal stress, increase in shear stress, or change in pore pressure – all of which can cause a fault to rupture (Ellsworth 2013). Studying the stresses from any of these triggering mechanisms provides an opportunity to understand the nature of stress and faulting.

Dynamic triggering has been shown to occur often (e.g., Velasco et al. 2008; Prejean et al. 2004; Wei et al. 2018), and we can study this phenomenon as a tool to systemically probe faults to address fundamental physical mechanisms of faulting. However, the underlying mechanisms that control dynamic triggering remain relatively uncertain and may provide the understanding needed to accurately evaluate earthquake probability (Brodsky and van der Elst 2014). Dynamic, sometimes referred to as remote, triggering can occur either locally (Fan and Shearer 2016) or thousands of kilometers away from the mainshock (Stein and Liu 2009). Dynamic triggering can

also occur as near-instantaneous or delayed events. Delayed triggering manifests as an increase in seismicity rate in the following weeks or months after the passage of the surface wave (Belardinelli, Bizzarri, and Cocco 2003; Gonzalez-Huizar et al. 2012). Alternatively, near-instantaneous triggering occurs during the passage of the seismic waves – usually during the *S* or surface wave train from large magnitude events (Velasco et al. 2008).

In this paper, we focus on identifying and analyzing dynamic triggering in the state of Utah following 227 $M \geq 7$ earthquakes that have occurred from 2000 through 2017 – we will refer to these as "mainshocks." We identified and investigated high-frequency signals that indicate local triggering. We divide our study into three analyses: a catalog analysis, a manual detection analysis, and an automatic detection analysis. From these efforts, we illustrate the appropriateness and relations between each analysis. In all cases, we investigate quantitative changes in seismicity and associations with other events to identify dynamic triggering – similar to prior studies (Velasco et al. 2008; Linville et al. 2014). The relatively high coverage of seismic stations and a sizable amount of catalogued local events made Utah an ideal location for studying dynamic triggering. Furthermore, there have already been confirmed instances of dynamic triggering recorded in Utah (Pankow et al. 2004).

Dynamic Triggering

When a fault ruptures, it generates acoustic waves in the ground that propagate through the Earth as seismic body and surface waves. Body waves (i.e., P waves and S waves) travel through the body of the Earth, and surface waves (i.e., Rayleigh and Love waves) move along the surface of the Earth. While all phases have the potential to be destructive, surface waves tend to be more damaging due to their large amplitudes and strain that they exert on the ground – causing sizable temporary deformations of the surface. Past studies have shown that surface waves can also travel thousands of kilometers triggering earthquakes across the globe and, thus, lead to additional damaging events (Kanamori 1972; Hill et al. 1993; Brodsky, Karakostas, and Kanamori 2000; Prejean et al. 2004; Gonzalez-Huizar et al. 2012).

Ever since 1992 (i.e., after the first confirmed instance of dynamic triggering), seismologists have detected and studied dynamic triggering in over 30 major earthquakes (Brodsky and van der Elst 2014). The 1992 Landers earthquake provided the first observed instance of dynamic triggering (Hill et al. 1993); this incited the examination of dynamic stresses as a potential source for remote seismic triggering. Other notable instances that displayed dynamic triggering include the 1999 M 7.1 Hector Mine earthquake in California (Gomberg et al. 2001), the 2002 M 7.9 Denali earthquake in Alaska (Prejean et al. 2004), and more recently the 2016 M 7.8 Kaikoura earthquake in New Zealand (Warren-Smith et al. 2018). The 2002 Denali M 7.9 earthquake in particular is relevant to our study as it is the most notable instance of remote triggering in Utah. In the period after the surface wave arrival, a past study observed a > 10 times increase in seismicity during the first 24 hours and continued to show increased seismicity for the following 24 days. The study also showed that most triggered events occurred along the major normal faults in the region including along the Wasatch fault. Triggered Utah events were reported in many instances appear as aftershocks in the region and possess magnitudes that range from less than 0 to 3.2 (Pankow et al. 2004).

Following the discovery of dynamic triggering, scientists have proposed various mechanisms for these dynamically triggered events including processes related to changes in Coulomb failure, rate-state friction, viscous fault creep, subcritical crack growth, and various others (Brodsky and Prejean 2005; Brodsky and van der Elst 2014). Although a combination of these mechanisms can offer some reasonable explanation on how seismic triggering occurs, there has been little consensus on what truly drives this phenomenon. Figure 1.0 illustrates how permanent and transient changes in stress related to triggering can promote premature fault failure in a very general sense.

Tectonic Setting

Utah is located in a seismically active region governed by extension and some volcanic activity. The Utah region can be divided into three major tectonic provinces; from southeast to northwest lies the Colorado Plateau, Middle Rocky Mountains, and the Basin and Range province. The Colorado Plateau province in the southeast to east regions of Utah is distinguished by a less tectonically active region with relatively smooth topography. The Middle Rocky Mountains province in the northeast is a region with mountainous terrain formed from the west-dipping Wasatch normal fault. West of the Wasatch Fault lies the Great Salt Lake in the Basin and Range province which is surrounded by other major faults that form the northern trending mountain ranges in the region (Hecker 1993). The southwestern regions of Utah also contain Quaternary volcanic vents as old as 170 years (Valastro, Davis, and Varela 1972). Overall, the region is dominated by normal faults that dip towards the west (see Figures 1.1 and 1.2). Most of the seismicity in the region is characterized by shallow (i.e., depths >15 km) normal with a strike-slip component earthquakes (Smith and Sbar 1974).

Data

Catalog

During our catalog analysis, we used the United States Geologic Survey (USGS) catalog to construct a list of mainshock events with M ≥ 7 that occurred within 2000 to 2017 – totaling to 276 mainshocks. We obtained data from the USGS catalog by using the USGS Search Earthquake Catalog web service and includes earthquakes throughout the globe. The USGS catalog is an accumulation constructed using various seismic networks and provides a reliable list of all large magnitude (> 6 M) earthquakes. However, USGS reports that this catalog should not be relied on as a complete list for all earthquakes within the United States with varying levels of completeness for lower magnitude events ("ComCat Documentation - Data Availability" 2019). For this reason, we choose not to use this catalog for our local catalog analysis.

Instead, we used the University of Utah Seismic Station (UUSS) catalog to compile a list of all local Utah events for evaluating the occurrence of remote triggering in Utah. Specifically, we use UUSS digital catalog that contains earthquakes from 1981 to 2018 that complete for magnitudes above 1.5 – 3 depending on the area ("Quality and Completeness of UUSS Catalog Data: 1981-Present | U of U Seismograph Stations" n.d.). The UUSS catalog was constructed using 55 to 175 stations maintained by UUSS. Identified detections related to quarry blasts are removed from this catalog (Arabasz, Pechmann, and Burlacu 2016). The UUSS catalog was obtained from the UUSS Earthquake Catalogs web page and includes earthquakes that occurred in the Utah and Yellowstone region. For the purposes of our study, earthquakes that contained a latitude between 36° and 42.5° and longitude between -115° and -108.5° were considered local Utah events; a total of 33,634 recorded events were specified for our period within this area.

Waveforms

Our waveform data consisted of 3-component (i.e., East, North, and vertical "Z" component) seismograms provided by broadband and high-broadband channels from 101 stations. Stations included 63 from EarthScope's Transfer Array (TA), 3 from United States National (US),

and 35 from University of Utah Regional (UU) networks located in the Utah region. For each mainshock, we acquired waveform data from the ±5 hours encompassing the mainshock arrival. Figure 1.1 contains a map showing the location of these stations. All waveform data was collected from the Incorporated Research Institutions for Seismology (IRIS) Data Management Center using Standing Order for Data (SOD) software provided by the University of South Carolina. We used the Antelope Software package by Boulder Real Time Technologies, Inc to construct a database and visually interact with the collected waveform data.

Station Seismic Noise Analysis

We removed noisy seismic stations (stations that display instrument and anthropogenic noise) from our dataset by evaluating Daily Probability Density Functions (PDF) Mode plots for each seismic station. The Daily PDF Mode Timelines that evaluates 0.010 Hz to 9.870 Hz frequency response at each station over the past three years were obtained from IRIS's MUSTANG data quality metrics web service (Casey et al. 2018). We analyze noise levels at 0.100 Hz and 9.870 Hz at each seismic station to determine if a station is recording excessive seismic noise. Stations that demonstrated consistently higher power 9.870 Hz frequencies relative to 0.1 Hz frequencies likely indicated high amounts of natural, anthropogenic, or instrumental noise (Casey et al. 2018; McNamara and Buland 2004). We omitted stations classified as noisy from our analyses in order to remove skews in our results. Figure 1.3 displays an example of two stations, one with negligible and another with large amounts of apparent high-frequency noise.

Methodology and Results

Statistical Approach to Triggering

We use a statistical threshold and a "special case" evaluation to determine if a mainshock has dynamically triggered earthquakes in Utah. First, we calculate the average number of events occurring within the five hours before the mainshock arrival ($Npre_{avg}$). We then calculate the probability of events for a Poisson distribution using the following equation

$$P(k) = \left(e^{-\lambda_i}\right)\frac{\lambda_i^k}{k!} \quad (1)$$

$$\text{given } k = \begin{cases} Npre_i & Npre_i > Npre_{avg} \\ Npre_{avg} & \text{otherwise.} \end{cases}$$

where $Npre_i$ and λ_i are equal to the number of events occurring before and after mainshock *i*, respectively; for example, our manual detection possessed an average background seismicity of 3.52 (with a standard deviation of 4.64) events. To simplify our calculation, we round-up to the nearest whole number and thus, set $Npre_{avg}$ equal to 4 for our analysis. We then classify a mainshock as triggering if we observe a 95% certainty of triggering (i.e., about a 5% chance of occurring "naturally") using Equation (1) given an increase in seismicity following the mainshock arrival – a method employed in similar studies (Linville et al. 2014; Velasco et al. 2008; Pankow et al. 2004; Brodsky, Karakostas, and Kanamori 2000). Given the information above and that $Npre_{avg} > Npre_i$, we determined that mainshocks that produce at least 9 local earthquakes after the mainshock arrival are considered triggering events.

We identified special cases as events with a non-significant increase in seismicity that contain local earthquakes during the passage of the S wave or a surface wavetrain. We verified all events in this category as containing a local event occurring during the passage of said phases.

Catalog Analysis

Utilizing the UUSS catalog, we extracted local earthquakes that occurred within 5 hours from the arrival time of the 276 mainshocks; a total of 754 local events occurred during the 10-

hour windows. We evaluated these events to determine which earthquakes show indications of being statistically triggered using a Poisson probability evaluation.

From the catalog analysis, 5 mainshocks exhibited seismicity increases indicative of dynamic triggering. A total of 81 local Utah events appeared triggered as a consequence of these mainshocks. In order to evaluate the regions catalogued seismic activity, we solved for the seismic moment (M_0) using the following equation

$$M_w = \frac{2}{3}\log_{10}(M_0) - 10.7 \qquad (2)$$

$$M_0 = 10^{\left(\frac{3}{2}(M_w+10.7)\right)}$$

by using the moment magnitudes (M_w) provided by the UUSS catalog. We binned each catalogued event using a grid with 0.1-degree grid spacing and summed the seismic moment to estimate the overall seismic moment experienced for a given area. We then applied a kriging interpolation using the summed seismic moment to construct a moment map of Utah. Due to a wide range of the calculated summed moment, we plotted $\log_{10}(M_0)$ and capped the value at 4000 newton-meters for our final moment heat map, Figure 1.4. The map shows north to south trend with an increased seismic moment with a significant increase in east-central Utah. The significant peak contains moments of some of the larger (M ~4) earthquakes in the region along with a significant number of small events.

Automated Waveform Detections

Due to the limitations on the UUSS catalog data, the catalog results likely provides an inaccurate analysis of the triggering in the area (Arabasz, Pechmann, and Burlacu 2016). To evaluate and supplement this limitation, we employed a short-term average (STA) to long-term average (LTA) ratio detector on the waveform for all 276 mainshocks at a 5 Hz high-pass. We then removed detections that appeared in only one component of the seismograms within a one-second buffer – a method shown to minimize the inclusion of false positives (Velasco et al. 2016). Similar to the manual analysis, signals were then further categorized into pre/post-events.

As noted, we obtained an average signal detection of 161 local pre-events for five hours; we remain apprehensive about the occurrence of such a large number of earthquakes transpiring within a relatively short time. Thus, we suspect a significant number of false positives and emphasize that the automated detections do not provide a reliable indication of actual triggering. Instead, we assume that false positives affect both pre-event and post-event counts similarly; thus, allowing for a relatively accurate assessment of the overall trends and deviations in seismicity caused by actual local earthquakes. Although such an analysis cannot provide a genuinely quantitative result of the triggered seismicity, it offers a suitable estimation of areas susceptible to dynamic triggering in Utah when compared to our manual analysis.

From the automated waveform analysis, 108 large magnitude mainshocks presented indications of potential triggering with a 95% certainty. From these, 89 mainshocks exhibited a 99% certainty of potential triggering. Given that using a 95% certainty for this analysis indicated that all mainshocks that contain a higher number of post-events and likely false positives, we decided that it would be more appropriate to conduct our analysis on the mainshocks with a 99% certainty of triggering. Due to the inconsistency of calculating surface wave arrival times automatically, we only categorized events into pre/post-events; thus, no special cases were considered. The pre-event average was 161 events with a standard deviation of 192.63. Figure 1.5 illustrates a triggering heat map constructed in the same fashion as the manual detection triggering heat map using the 99% certainty threshold. The automatic detections heat map displays a northwest to the southeast trending region of detected potential triggering. There also exists another seemingly isolated region of potential triggering in the southwest corner of Utah.

Manual Waveform Detections

In order to provide a more precise examination of the occurrence of triggering, we opted to examine earthquakes that contained a least a two-to-one increase in local seismicity following the mainshock. This method ensured that we included all statistically triggered events as well as potentially missed triggered events. Thus, we determined which events from the mainshock

cataloged contained at most half the number of pre-events relative to the number of post-events (i.e., earthquakes occurring before and after the mainshock arrival respectively). We treated all mainshocks as having at least one pre-event in order to include mainshocks with zero pre-events during this evaluation. A total of 65 mainshocks met the two-to-one threshold.

The visual examination involved manually inspecting the waveform data for the 10 hours encompassing the 65 mainshocks provided by the available stations. We aimed to compile a more comprehensive earthquake catalog of the region. We accomplished this by inspecting the entire waveforms from the available stations for each mainshock and identifying local earthquake signals. We utilize a 5 Hz high-pass filter during this process and, on occasion, also employed 1-5 Hz bandpass filter to aid in seismic signal identification. Figure 1.6 illustrates the benefits of using these filters; in this Figure, station NLU from the UU network shows the occurrence of multiple local events that are masked by the M 7.2 Northern Sumatra 2012 mainshock wavetrain. By applying a 5 Hz high-pass filter, local signals appear readily identifiable as spikes in the waveform. A closer inspection reveals that many of these signals are characteristic of local earthquakes. In Figures 1.6b and 1.6c, we show the occurrence of a pre and three post events, respectively, all of which have been catalogued by UUSS. Many of the relatively larger and prominent local earthquakes have been catalogued by UUSS. However, Figure 1.7 demonstrates an example of an event missing (potentially due to it possessing a low magnitude) from the catalog which we aimed to supplement for our visual analysis.

We also calculated average phase arrival times for these mainshocks and then categorized local event occurrence based on their arrival time relative to the phase arrivals. The two main categories include, pre-events and post-events, with the latter further divided into five subcategories: P-S events (i.e., events occurring between the *P* and *S* phases), S-L events (i.e., events occurring between *S* and Love phases), L-R events (i.e., events occurring between Love and Rayleigh phases), R-D events (i.e., events occurring during Rayleigh coda), and Delayed events (i.e., events occurring after the mainshock coda).

We determined that of the 276 large magnitude mainshocks, 23 events were involved in the dynamic triggering of local earthquakes in the Utah region. Table 1.0 includes a list of these events and Figure 1.8 shows a map of all mainshocks, marking those involved in dynamic triggering with a white star. We find 268 local events were triggered in the study area – 55% of which were previously uncatalogued. From these events, 66 were instantaneously triggered by Rayleigh waves, 5 Love Waves, 28 S waves. The remaining local earthquakes were triggered after a delayed period following the mainshock coda. In order to infer a general location of the uncatalogued triggered events, we plotted a heat map based on the station locations and the number of triggered events captured, see Figure 1.9. The map displays an increase in triggering detections from the Great Salt Lake in the northwest and continues to southeast with a few isolated areas scattered in the northeast and southwest parts of Utah. The largest amount of detected triggering occurs within central Utah.

Discussion

While we aimed to use all of the data available, we omitted several problematic datasets. During the manual detection analysis, we removed detections from station P18A from the TA network due to regular intervals of ostensibly anthropogenic seismic activity. This assumption was supported upon further examination revealing a mining site approximately 15 km southwest from this station. Furthermore, the station exhibits regular (seemingly anthropogenic) increases in seismic activity during 6:00 - 9:00 AM for the 65 manually inspected mainshocks, see Figure 1.10. Including data from this station offered the additional challenge of distinguishing local earthquakes from numerous potentially anthropogenic-related waveform signals (e.g., quarry blasts or induced seismicity) that are outside the scope of this project; for this reason, we omitted picks from this station to prevent skews from anthropogenic activity in our results (Velasco et al. 2016). Some mainshock analyses were also limited to using catalog data exclusively due to the quality or absence of the available waveform data; these were a consequence of limited data that contained significantly noisy or patchy recordings (i.e., missing over 25% of a waveform recording). The following 7 mainshocks fell in this category: 2000 Turkmenistan M 7.0, 2000 Japan M 7.6, 2000 Jujuy, Argentina M 7.2, 2000 Southern Sumatra M 7.9, 2001 Vanuatu M 7.1, 2001 Molucca Sea M 7.1, and 2002 Denali M 7.9 earthquakes.

We also investigated the occurrence of triggered events to assess if there existed any bias based on our data coverage. Figure 1.11 shows a histogram based on the data from our manual analysis. We found that the data coverage shows relatively negligible bias towards any given time but shows some hours of higher triggered earthquake occurrence. The observed higher counts during the afternoon hours may indicate that some of the triggered events are related to anthropogenic activity mistaken as naturally occurring earthquakes. However, when considering the verified catalog events, we see a similar trend that perhaps suggest that this may be characteristic of the region's triggering. Nevertheless, in future work, quarry blast data should be utilized to omit potentially mistaken triggered events.

The catalog analysis provided a lower estimation of the triggering, which is likely related to the UUSS catalog's magnitude threshold. During this analysis, only 5 mainshocks displaying any significant statistical increase in seismicity indicative of dynamic triggering. Given our result from the manual detections, we identified a number of events below the catalog's magnitudes completeness, making it difficult to identify dynamic triggering in Utah. The requirement to locate an event is to have, at a minimum, 4 observations; thus, although Utah's catalog provides an exception regional catalog for small magnitude events, the catalog offers a complete list of events with 1.5 - 3.0 magnitudes – as mentioned in the catalog data section. Our approach of looking at single stations is able to detect events below this threshold. Given that we only examined 65 mainshocks, the catalog showed that 230 local events occurred the 10-hour window while our visual inspection revealed a total of 614 local events; likewise, 81 of the catalog events were considered triggered versus the 268 of the visually detected triggered events. This suggests that our uncatalogued earthquakes are well below the UUSS catalog inclusion threshold (i.e., in relation to magnitude).

From our heat maps, we observe some striking correlations that could provide some perceptive on the regions triggering and the reliability of each of our analyses. In Figure 1.4, we highlight the area displaying the highest amount of experienced seismicity (red dashed outline). By comparing the location and shape of this occurrence to the other maps, we find that all maps have a shared northwest to southeast region of high activity. However, the manual detections show the largest amount of triggering occurring within central Utah just northwest from the region experiencing high accumulative seismic moment; thus, suggests that areas with high seismic moment are not necessarily prone to remote triggering. In contrast, the automatic detections map does have its highest peak within the area of high seismic moment. We speculate that although there likely exists some relation between moment and the amounts of events experienced in an area, dynamic triggering not dependent on areas experiencing these characteristics. When comparing the manual and automatic heat map we notice a meaningful amount of agreement. We propose that the STA/LTA detection used and Poisson analyses conducted, provide a suitable

proxy for highlighting areas susceptible to dynamic triggering. Yet, the maps do express some notable differences (e.g., the southwest segment of Utah shows considerably higher indication of triggering in the automatic detections map). Without a complete manual analysis of all mainshocks, we cannot confidently say these are an artifact due to false positive detection or a large sequence of triggered events not included in our visual detection analysis. However, such an automated process may be sufficient and ideal for processing larger datasets (i.e., examining triggering susceptibility or potential occurrence for the entirety of the United States).

Finally, the heat maps we constructed on their own provide a reasonable backdrop to areas that experience triggering but offer little enlightenment on the manifestation of these events. To supplement this, we obtained the back azimuth for all mainshocks and plotted this data onto a stress map of the Utah region using our manual detection results, see Figure 1.2. Note that back azimuth lines (black) are plotted based on station locations for stations that captured a triggered event during a given surface wave; this was done to compensate for the lack of local earthquake locations for many of our detections. From this examination, we observed that most surface waves approach the regional faults at a relatively perpendicular angle to strike. Specifically, most of the faults have a north-south strike orientation and see that most triggering sequences occur during the passage of east-west traveling surface waves. We hypothesize that during the passage of the surface waves, the faults experience strain that momentarily decouples the faults leading to the occurrence of a dynamically triggered earthquake. In future studies we suggest that the location for dynamically triggered uncatalogued earthquakes be determined and used to plot the back azimuths of the triggering mainshocks; this should provide a more accurate representation of the relationship that the surface waves have with the region's faults.

Conclusion

In this study, we identified dynamic triggering in the state of Utah following 227 global mainshocks with M ≥ 7 that occurred from 2000 to 2017. Our results showed that based on solely UUSS catalog data, only 5 mainshocks were involved in triggering Utah earthquakes. During our manual detections, we identified high-frequency signals that indicate local earthquakes for the 65 mainshocks that showed a two-to-one increase in seismicity; from this data, we determined that an additional 18 mainshocks were involved in dynamic triggering. We conducted an automatic STA/LTA detection on our dataset and found 89 mainshocks showed indications of triggering. The automatic detection analysis also revealed a striking resemblance in areas with relatively high triggering activity to those exhibited by the manual detection analysis. The catalog and visually detection results also revealed that a majority of the local events were missing from the UUSS catalog – a discrepancy likely due to these events having lower magnitudes than those included in the catalog. Finally, we observed that there seems to be some correlation between fault ruptures in Utah during the passage of surface waves that have a back azimuth relatively perpendicular to that of the fault's strike direction.

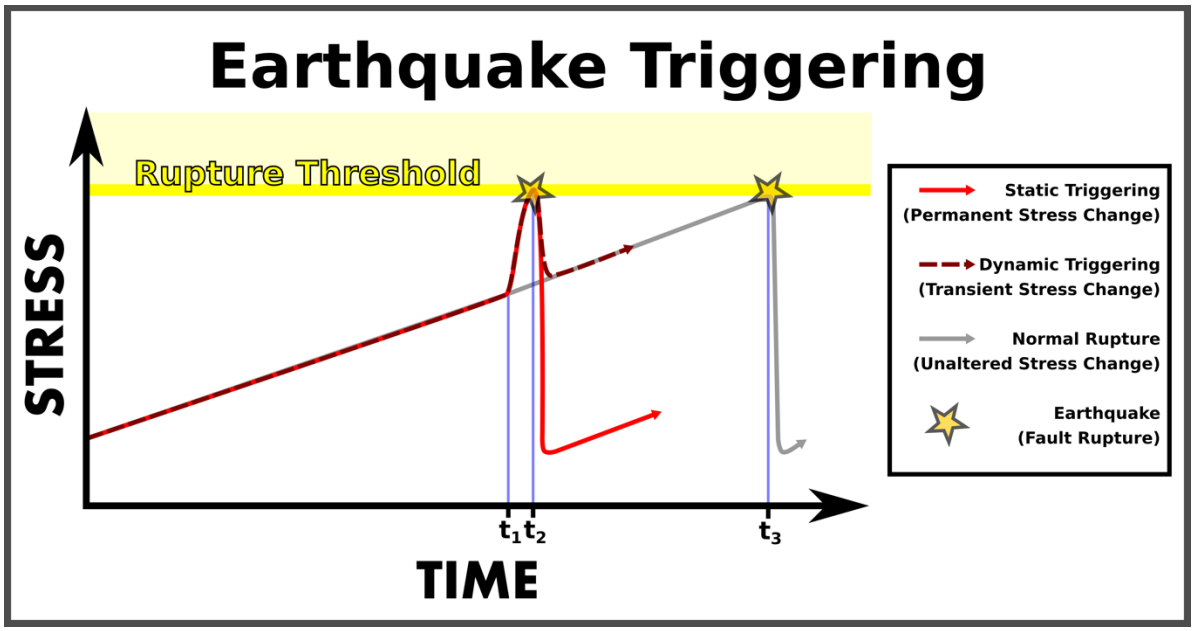

Figure 1.0: Illustration of the stress change relationship assumed for static (solid red line) and dynamic (dashed dark red line) triggering of an earthquake at t_2. For static triggering, t_1 indicates the time at which a permanent stress change occurs following a disrupted event (e.g., an earthquake on an adjacent fault). For dynamic triggering, t_1 represents the arrival of seismic waves from a separate large magnitude event. The gray line represents the stress change, if unaffected by external factors; thus, leading to fault failure at a later time (i.e., an earthquake at t_3).

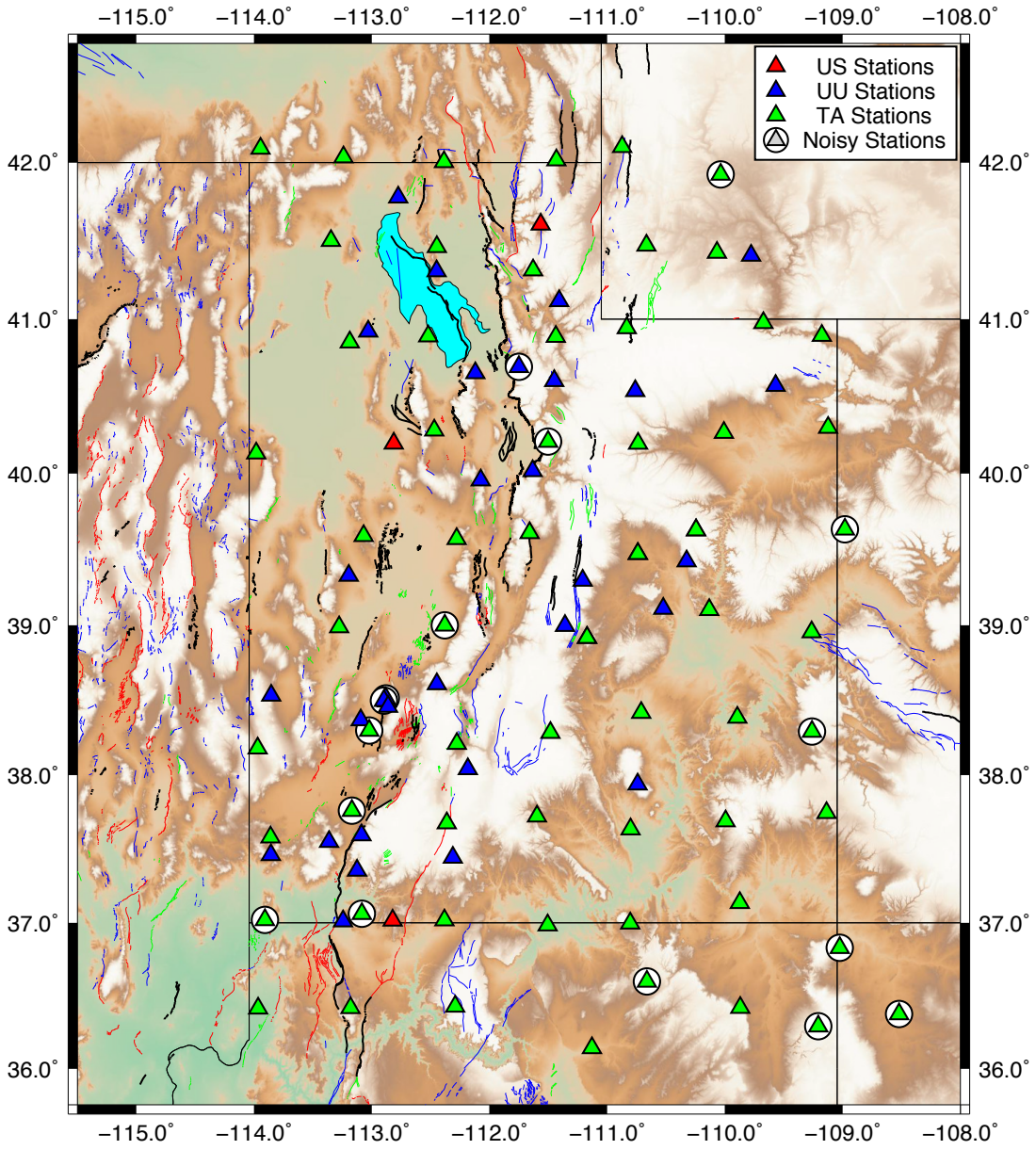

Figure 1.1: Map of Utah showing the location of the seismic stations from which we gathered waveform data. Stations consist of 63 Transportable Array (TA) stations, 3 United States National Network (US) stations, and 35 University of Utah (UU) Regional Network stations. Stations removed from the final analysis are enclosed with a white circled. Major faults and topography in Utah using the USGS classification for faults (USGS website). Thick black lines show Quaternary faults (<15,000 years) with well constrained location; Red lines show late Quaternary faults (<130,000 years) with moderately constrained location; Green lines show middle and late Quaternary faults (<750,000 years); Blue lines show undifferentiated Quaternary faults (<1.6 million years) that are well constrained in location.

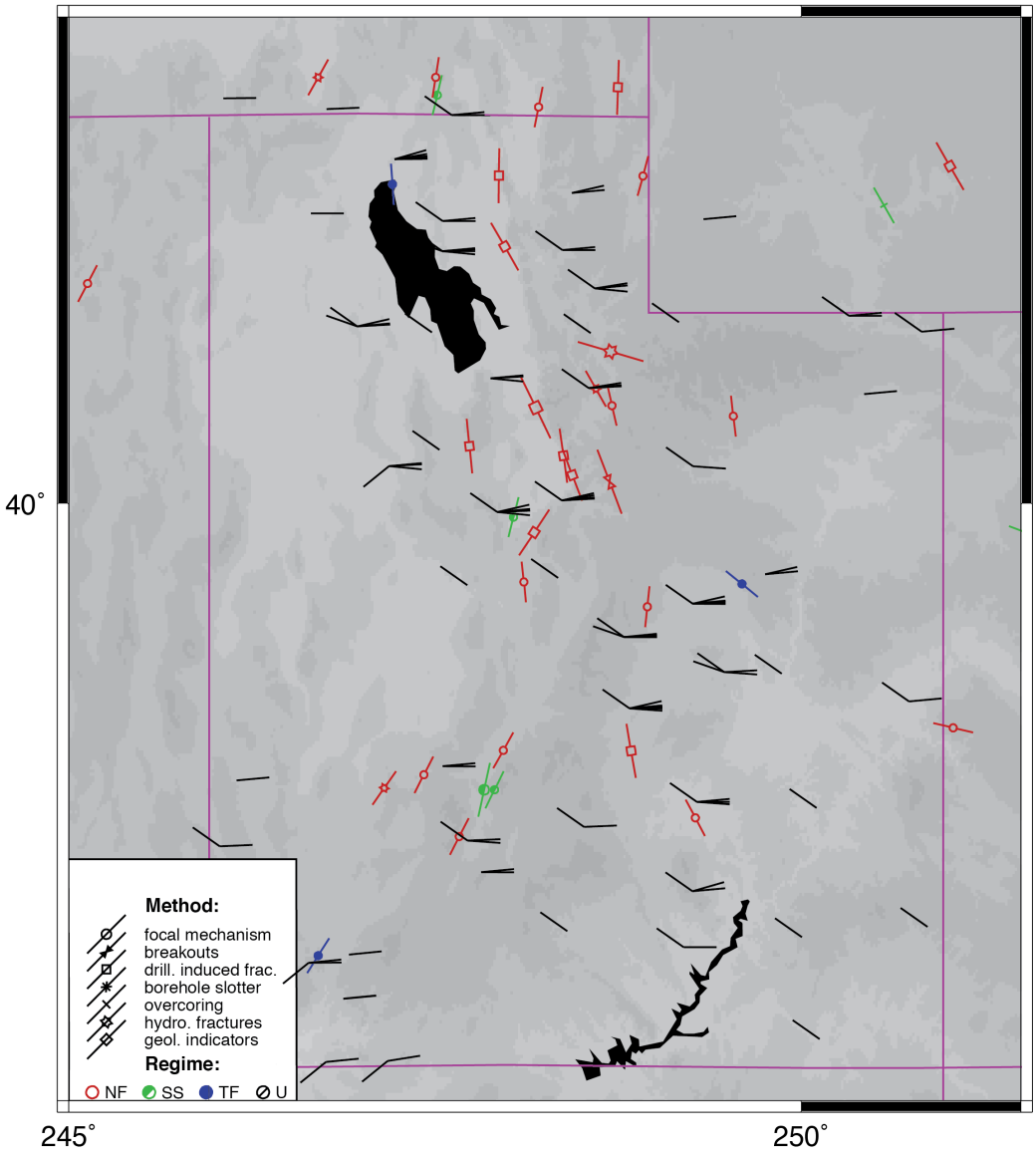

Figure 1.2: Stress map of Utah region with back azimuths (black lines) for triggering mainshock surface waves based on the location of the station that detected the event. Faults are represented as a line with a shape (i.e., Normal = Red and Empty Shape, Strike-Slip = Green and Half-Solid Shape, Thrust = Blue and Solid Shape, and Unknown = Black and Divided Shape) where lines are oriented towards strike and shapes are determined by method at which faults have been characterized.

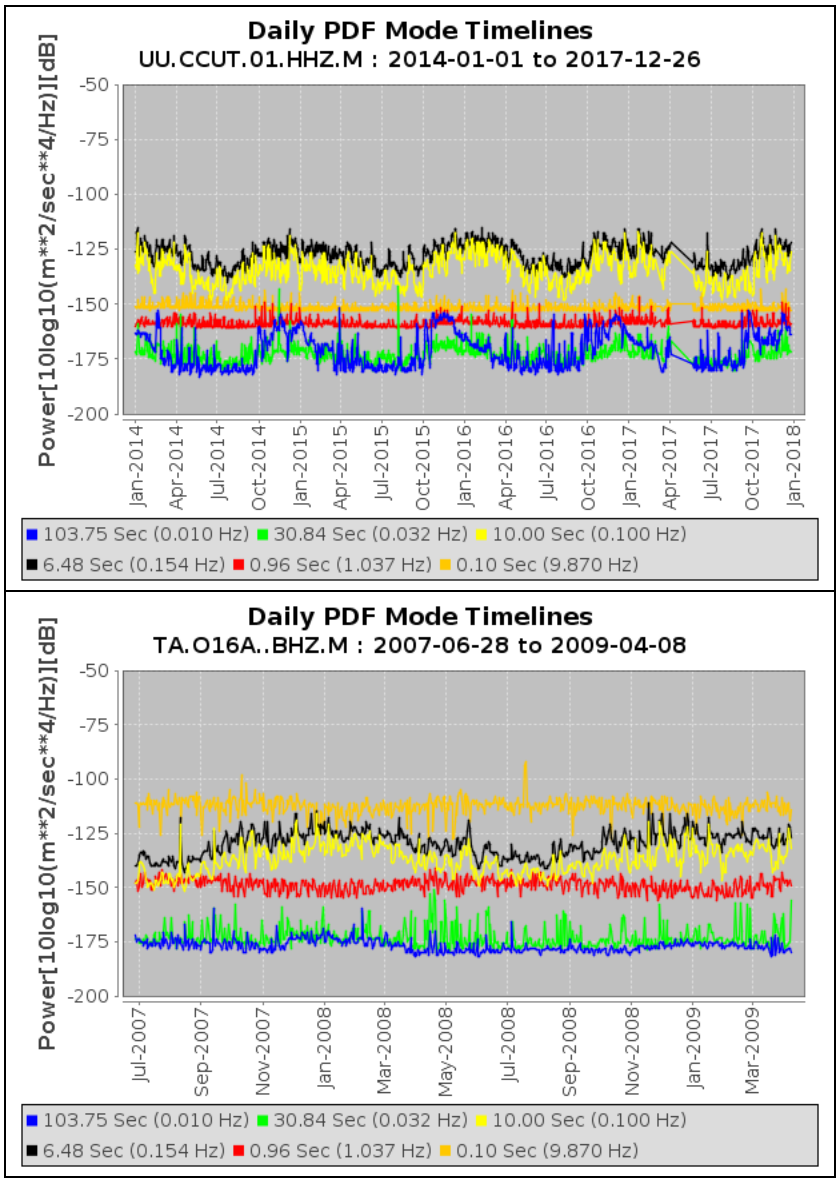

Figure 1.3: Daily Probability Density Functions (PDF) Mode plots obtained from IRIS's Mustang web service. The first (above) plot was obtained from station CCUT from the UU network and shows that the 0.10 sec period signals (yellow) are consistently lower power than the 10 sec period signals (orange) – suggesting that the high-frequency background noise will not mask the slightly lower frequency signals indicative of local events. In contrast, the second (below) plot shows that the 0.10 sec period signals have consistently higher power than the 10 sec period signals; such stations were thus removed from our final analysis due to their potential to mask local events.

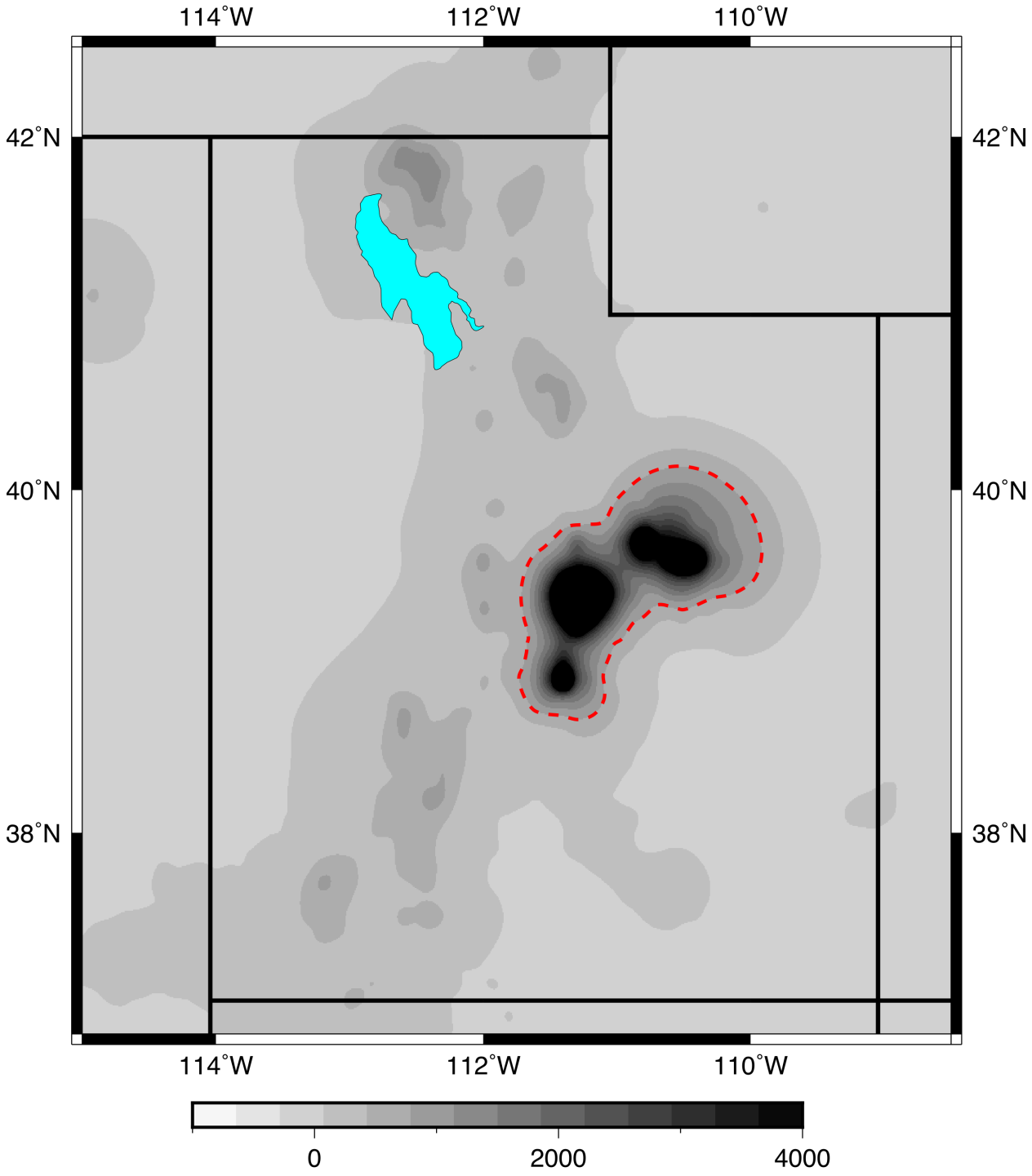

Figure 1.4: Heat map of the cumulative seismic moment of UUSS catalogued earthquakes. Red dashes outline an area with a significant overall experienced seismic moment.

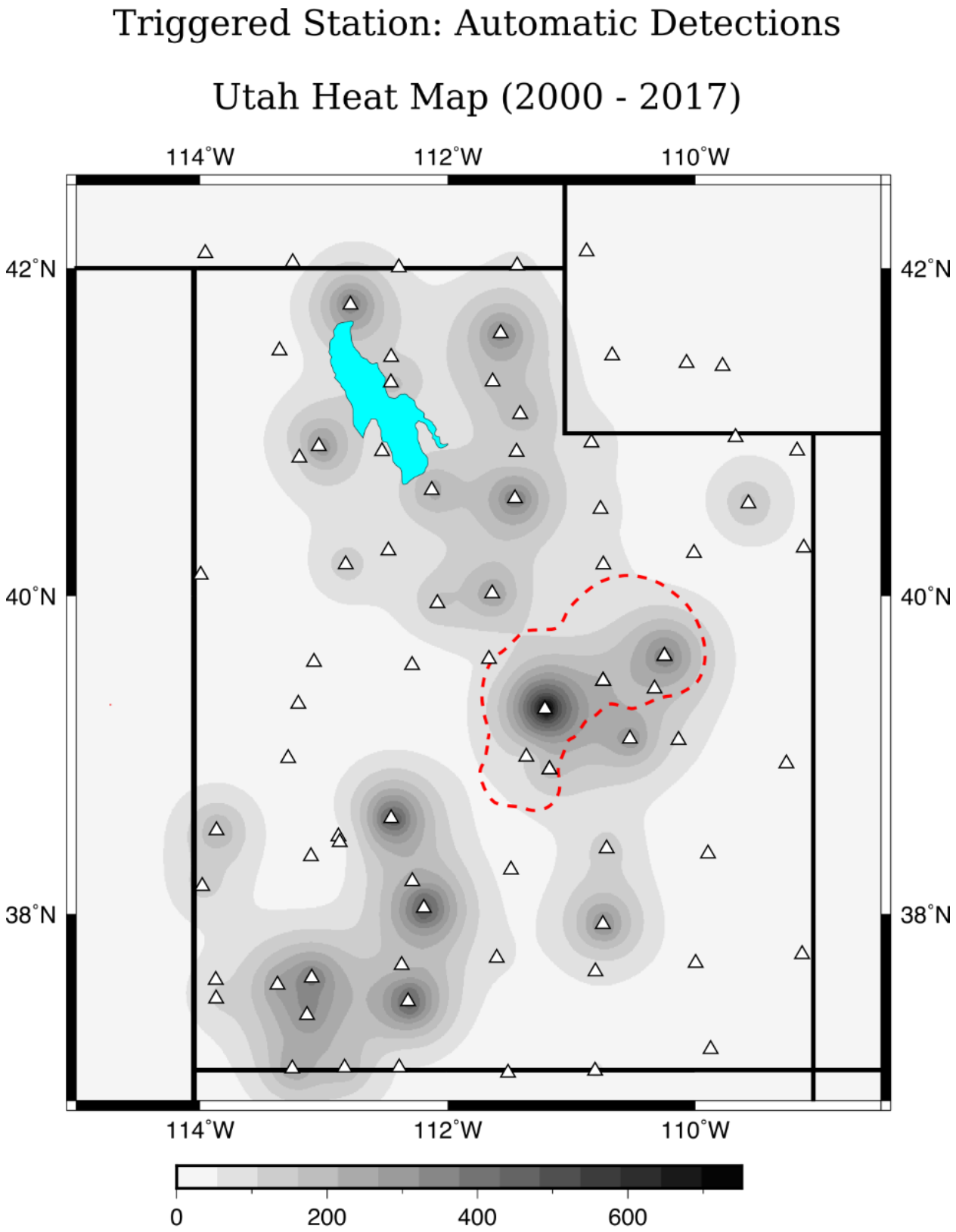

Figure 1.5: Heat map of dynamically triggered earthquakes plotted on station locations from which detections were observed during the automatic detection. Triangles show station locations.

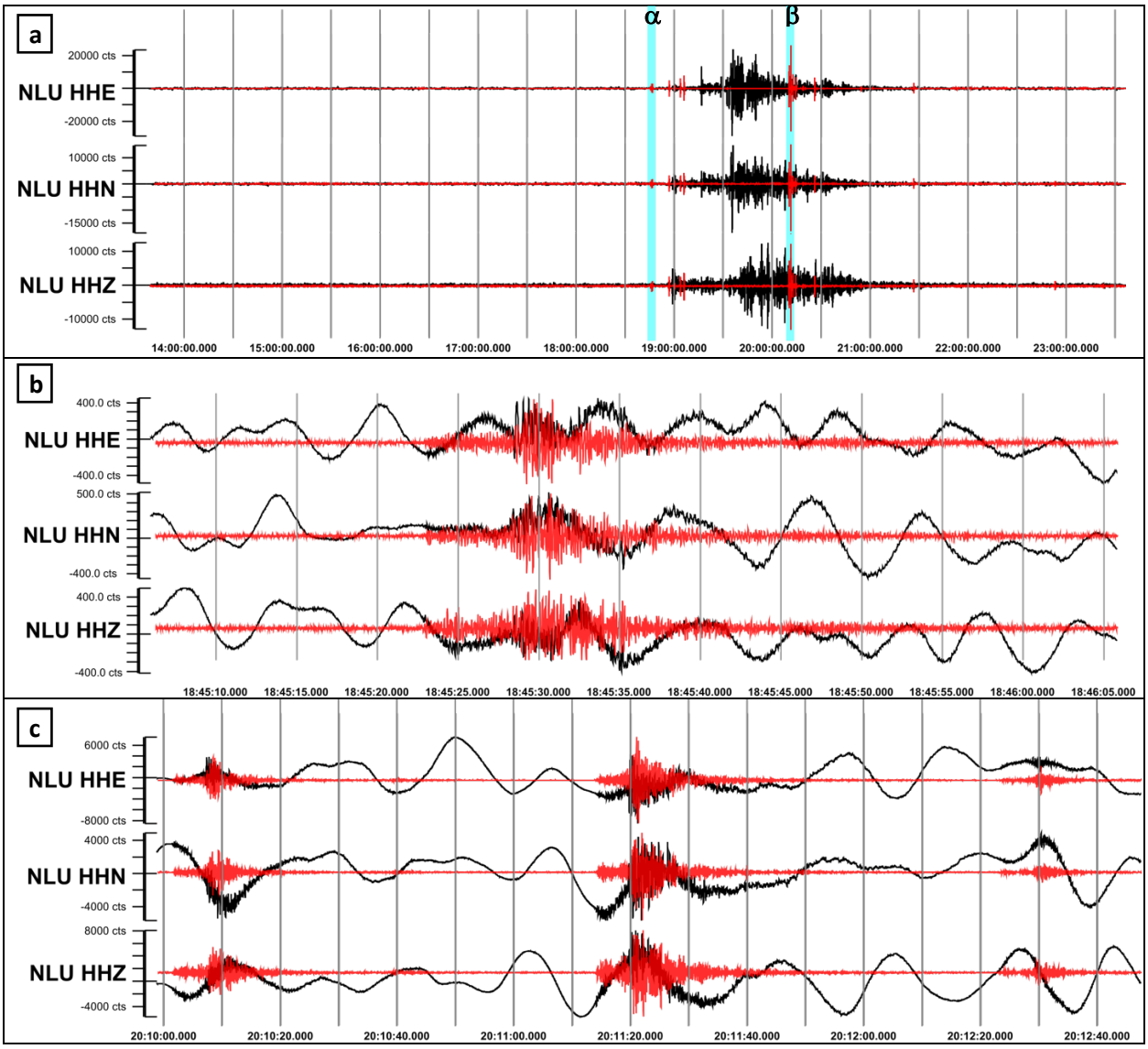

Figure 1.6: Three-component seismogram by station NLU from the UU network showing the passage of the M 7.2 Northern Sumatra 2012 earthquake; waveforms in black are recordings with no filter applied while those in red are the waveforms after a 5 Hz High-pass filter has been applied. Figure 1.6a display the entirety of the 10 hours collected for our analysis. Figure 1.6b is an enlarged view of segment α (highlighted in blue) as seen in Figure 1.6a that shows the occurrence of an earthquake occurring before the mainshock arrival. Similarly, Figure 1.6c is an enlarged view of segment β (highlighted in blue) that shows the occurrence of three dynamically triggered events occurring during the passage of the mainshock's Rayleigh wave.

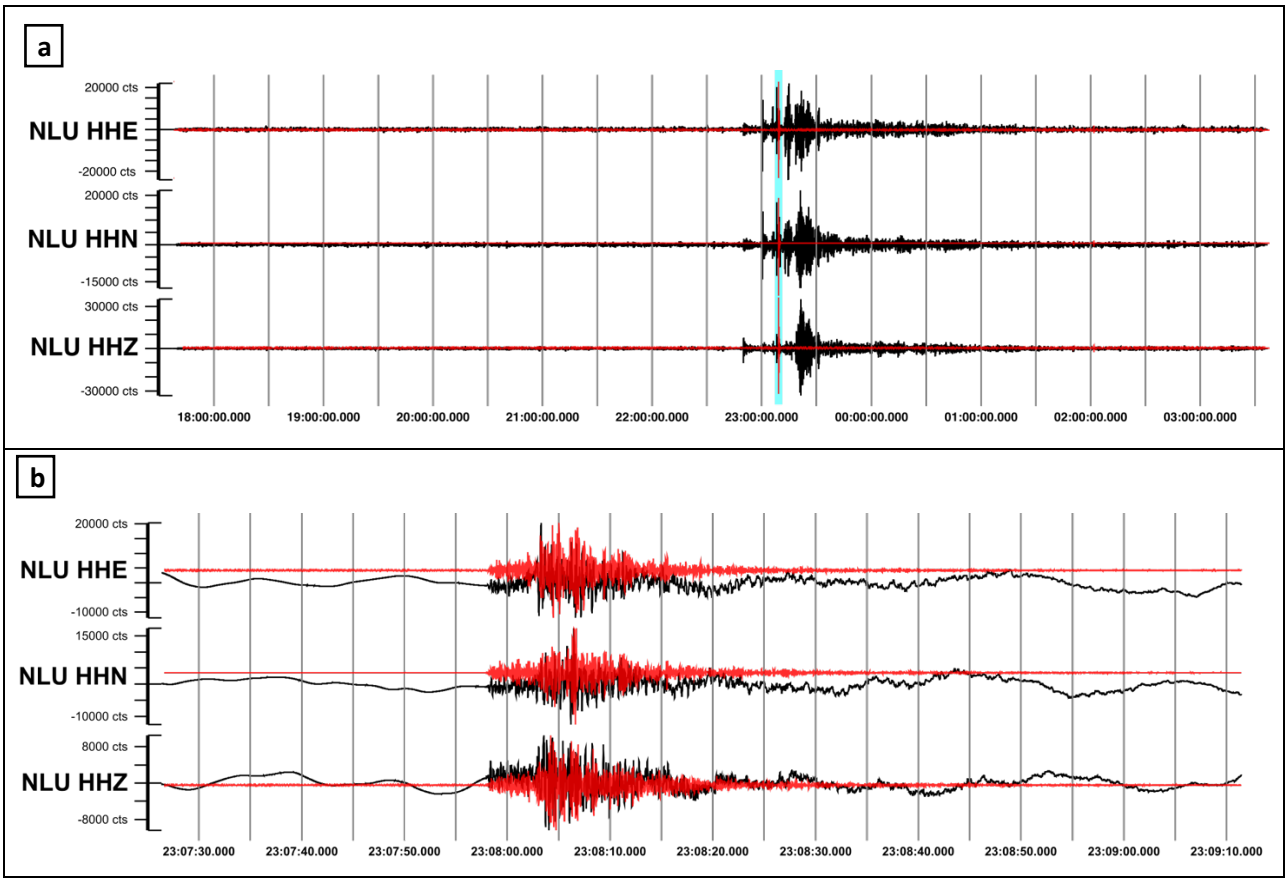

Figure 1.7: Three-component seismogram recording of the M 7.1 Maule, Chile 2012 earthquake by station NLU from the UU network; waveforms in black are recordings with no filter applied while those in red are the waveforms after a 5 Hz High-pass filter has been applied. Figure 1.7a display the entirety of the 10 hours collected for our analysis. Figure 1.7b is an enlarged view of the segment highlighted in blue and shows the occurrence of a triggered earthquake that has not been catalogued.

Table 1.0: Large Magnitude Triggering Mainshocks

Earthquake Location	M_w	Centroid Time, UT	Latitude (°)	Longitude (°)	Depth (km)	Δ (°)*	Class**
Tres Picos, Mexico	8.2	08 Sep 2017 04:49:19	15.02	-93.90	47.4	29.09	SC
Ile Hunter, New Caledonia	7.2	12 Aug 2016 01:26:36	-22.48	173.12	16.4	93.35	SC
Panguna, Papua New Guinea	7.1	11 Apr 2014 07:07:23	-6.59	155.05	60.5	96.44	SC
Maule, Chile	7.1	25 Mar 2012 22:37:06	-35.20	-72.22	40.7	82.88	SC
Northern Sumatra	7.2	10 Jan 2012 18:36:59	2.43	93.21	19.0	133.46	ST+
Kermadec Islands region	7.4	21 Oct 2011 17:57:16	-28.99	-176.24	33.0	90.96	SC
Kepulauan Mentawai region, Indonesia	7.8	25 Oct 2010 14:42:22	-3.49	100.08	20.1	133.54	SC
South Island of New Zealand	7.8	15 Jul 2009 09:22:29	-45.76	166.56	12.0	112.16	SC
Kermadec Islands region	7.0	18 Feb 2009 21:53:45	-27.42	-176.33	25.0	90.33	SC
Kepulauan Talaud, Indonesia	7.2	11 Feb 2009 17:34:50	3.89	126.39	20.0	112.49	SC
Papua, Indonesia	7.4	03 Jan 2009 22:33:40	-0.70	133.31	23.0	110.26	SC
Macquarie Island region	7.1	12 Apr 2008 00:30:12	-55.66	158.45	16.0	121.88	ST
Loyalty Islands, New Caledonia	7.3	09 Apr 2008 12:46:12	-20.07	168.89	33.0	95.48	SC
Simeulue, Indonesia	7.4	20 Feb 2008 08:08:30	2.77	95.96	26.0	131.17	ST
Kepulauan Mentawai region, Indonesia	7.9	12 Sep 2007 23:49:03	-2.63	100.84	35.0	133.78	ST
Molucca Sea	7.5	21 Jan 2007 11:27:45	1.07	126.28	22.0	113.54	SC
Taiwan region	7.1	26 Dec 2006 12:26:21	21.80	120.55	10.0	101.33	SC
Scotia Sea	7.6	04 Aug 2003 04:37:20	-60.53	-43.41	10.0	115.41	SC
Kuril Islands	7.3	17 Nov 2002 04:53:53	47.82	146.21	459.1	69.25	ST+
Denali National Park, Alaska	7.9	03 Nov 2002 22:12:41	63.52	-147.44	4.9	N/A	ST+
Guam region	7.1	26 Apr 2002 16:06:07	13.09	144.62	85.7	91.47	SC
Vanuatu	7.1	09 Jan 2001 16:49:28	-14.92	167.17	103.0	92.98	ST+
Turkmenistan	7.0	06 Dec 2000 17:11:06	39.57	54.80	30.0	99.82	ST+

Shaded earthquakes occur during deployment of seismic stations in Utah from the Transportable Array regional network.

* Great circle distance (Δ) values are based on average great circle distances from stations used during analysis.

**Classification for how the earthquake was considered to be dynamically triggering. (ST= Statistically; SC = Special Case; Events with "+" were also considered involved in dynamic triggering based on catalog analysis)

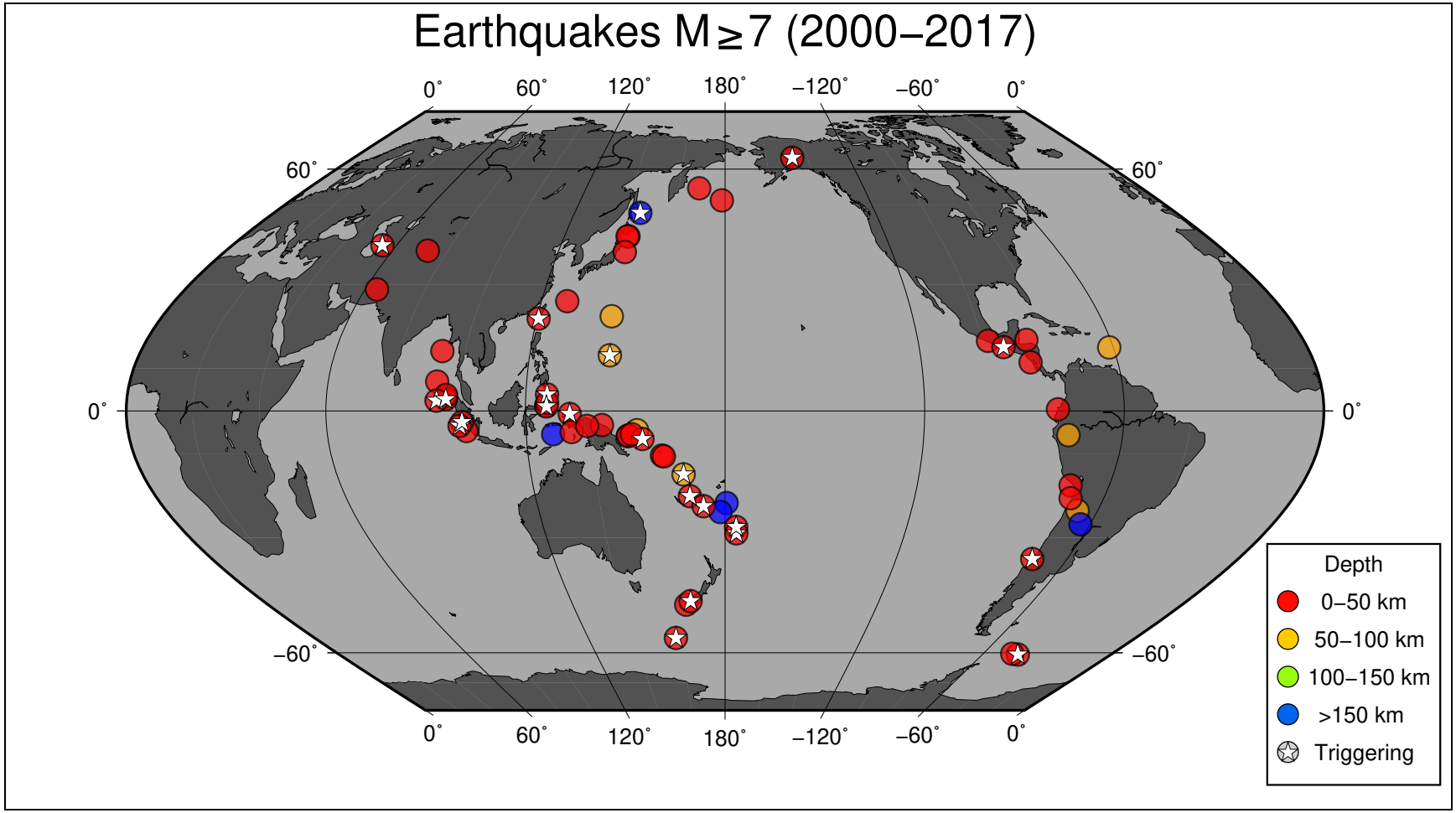

Figure 1.8: A world map of magnitude ≥ earthquakes (circles) colored by the depth at which the event occurred from 2000 to 2017. White stars indicate mainshocks involved in dynamically triggering events in Utah based on manual detections.

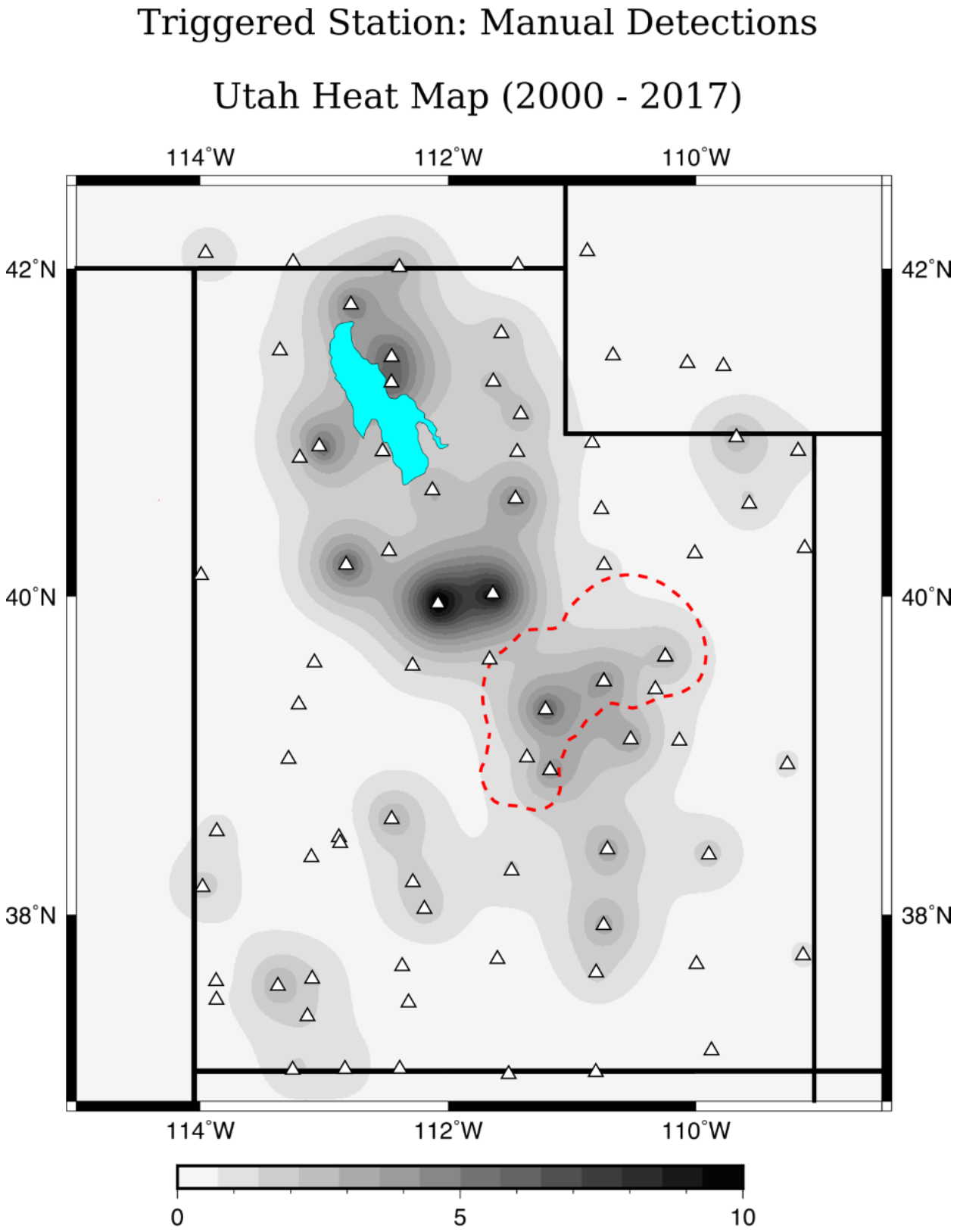

Figure 1.9: Heat map of dynamically triggered earthquakes plotted on station locations from which detections were observed during the manual review. Triangles show station locations.

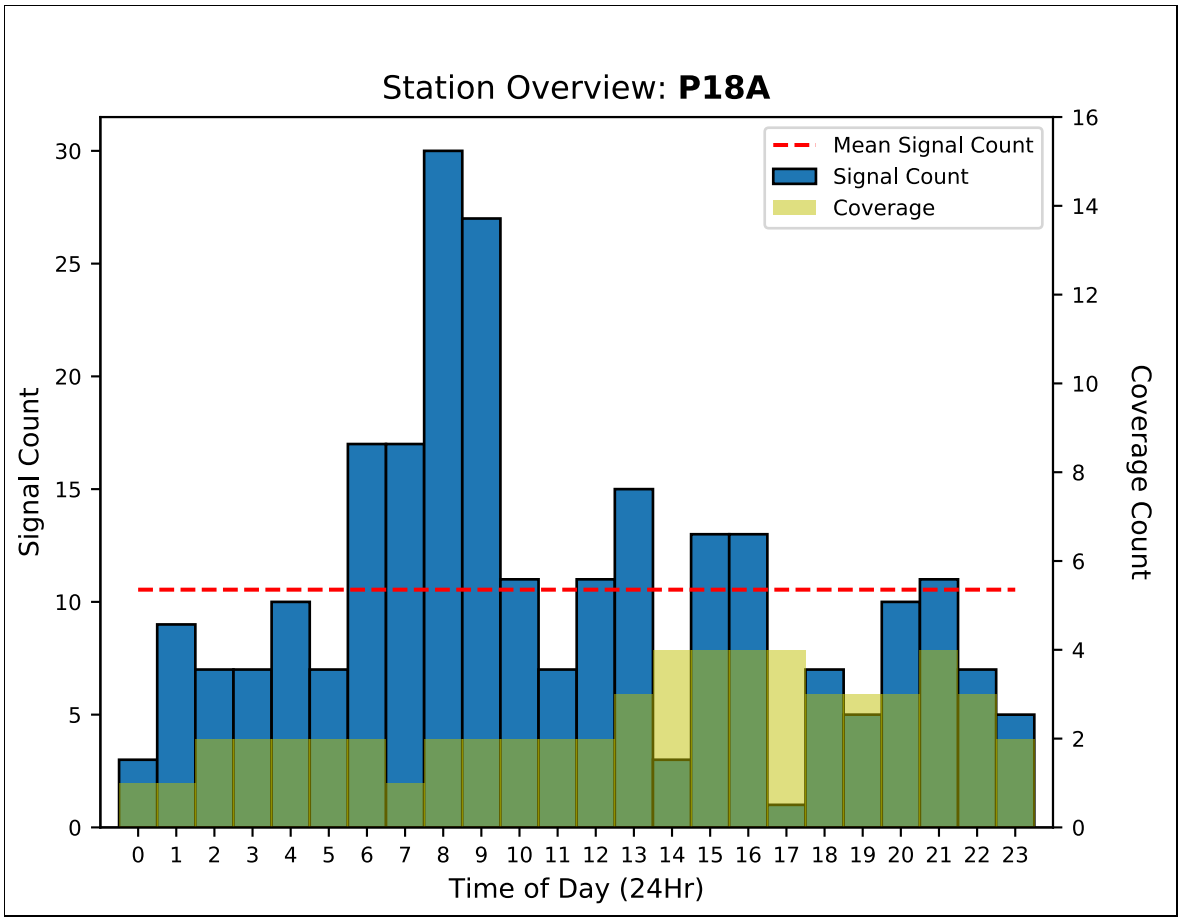

Figure 1.10: Histogram illustrating the hourly frequency of detected signals of station P18A from TA network based on the waveform data for the 65 manually reviewed mainshocks. The red dashed line is the average number of events detected. The transparent yellow bars indicate the overall coverage provide by the 10-hour waveform data used in this analysis. Signal detections were binned into hours of the day relative to local Utah time (Mountain Daylight Time, GMT -6 hours).

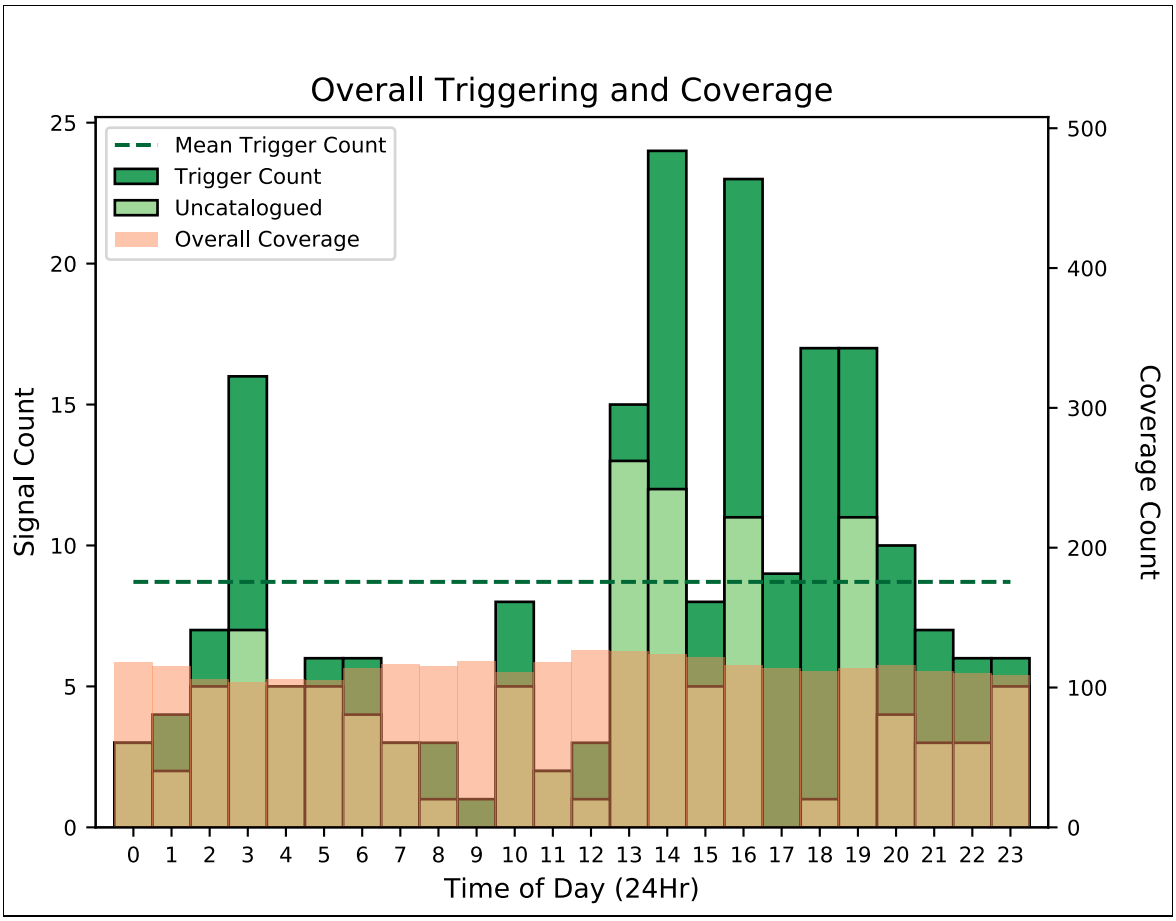

Figure 1.11: Histogram of triggered events relative to the hour they occurred using standard Utah local time (i.e., Mountain Daylight Time Zone). Dark green bars indicate the number of triggered events that were catalogued in the UUSS catalog. Light green bars indicate the number of uncatalogued triggered events. The green dashed line shows the overall (i.e., regardless of catalog status) average for the number of triggered events. The red transparent bars indicate the overall coverage provide by the 10-hour waveform data for each station recording.

References

Arabasz, Walter J, James C Pechmann, and Relu Burlacu. 2016. "A Uniform Moment Magnitude Earthquake Catalog and Background Seismicity Rates for the Wasatch Front and Surrounding Utah Region," 133.

Belardinelli, M. E., A. Bizzarri, and M. Cocco. 2003. "Earthquake Triggering by Static and Dynamic Stress Changes." *Journal of Geophysical Research: Solid Earth* 108 (B3). https://doi.org/10.1029/2002JB001779.

Brodsky, Emily E., and Nicholas J. van der Elst. 2014. "The Uses of Dynamic Earthquake Triggering." *Annual Review of Earth and Planetary Sciences* 42 (1): 317–39. https://doi.org/10.1146/annurev-earth-060313-054648.

Brodsky, Emily E., Vassilis Karakostas, and Hiroo Kanamori. 2000. "A New Observation of Dynamically Triggered Regional Seismicity: Earthquakes in Greece Following the August 1999 Izmit, Turkey Earthquake." *Geophysical Research Letters* 27 (17): 2741–44. https://doi.org/10.1029/2000GL011534.

Brodsky, Emily E., and Stephanie G. Prejean. 2005. "New Constraints on Mechanisms of Remotely Triggered Seismicity at Long Valley Caldera." *Journal of Geophysical Research: Solid Earth* 110 (B4). https://doi.org/10.1029/2004JB003211.

Casey, Robert, Mary E. Templeton, Gillian Sharer, Laura Keyson, Bruce R. Weertman, and Tim Ahern. 2018. "Assuring the Quality of IRIS Data with MUSTANG." *Seismological Research Letters* 89 (2A): 630–39. https://doi.org/10.1785/0220170191.

"ComCat Documentation - Data Availability." 2019. USGS. 2019. https://earthquake.usgs.gov/data/comcat/data-availability.php.

Ellsworth, William L. 2013. "Injection-Induced Earthquakes." *Science* 341 (6142): 1225942. https://doi.org/10.1126/science.1225942.

Fan, Wenyuan, and Peter M. Shearer. 2016. "Local near Instantaneously Dynamically Triggered Aftershocks of Large Earthquakes." *Science* 353 (6304): 1133–36. https://doi.org/10.1126/science.aag0013.

Freed, Andrew M. 2005. "Earthquake Triggering by Static, Dynamic, and Postseismic Stress Transfer." *Annual Review of Earth and Planetary Sciences* 33 (1): 335–67. https://doi.org/10.1146/annurev.earth.33.092203.122505.

Gomberg, J., P. A. Reasenberg, P. Bodin, and R. A. Harris. 2001. "Earthquake Triggering by Seismic Waves Following the Landers and Hector Mine Earthquakes." *Nature* 411 (6836): 462–66. https://doi.org/10.1038/35078053.

Gonzalez-Huizar, Hector, Aaron A. Velasco, Zhigang Peng, and Raul R. Castro. 2012. "Remote Triggered Seismicity Caused by the 2011, M9.0 Tohoku-Oki, Japan Earthquake." *Geophysical Research Letters* 39 (10). https://doi.org/10.1029/2012GL051015.

Hecker, Suzanne. 1993. *Quaternary Tectonics of Utah with Emphasis on Earthquake-Hazard Characterization*. Utah Geological Survey.

Hill, D. P., P. A. Reasenberg, A. Michael, W. J. Arabaz, G. Beroza, D. Brumbaugh, J. N. Brune, et al. 1993. "Seismicity Remotely Triggered by the Magnitude 7.3 Landers, California, Earthquake." *Science* 260 (5114): 1617–23. https://doi.org/10.1126/science.260.5114.1617.

Kanamori, Hiroo. 1972. "Relation between Tectonic Stress, Great Earthquakes and Earthquake Swarms." *Tectonophysics* 14 (1): 1–12. https://doi.org/10.1016/0040-1951(72)90002-9.

King, Geoffrey C. P., Ross S. Stein, and Jian Lin. 1994. “Static Stress Changes and the Triggering of Earthquakes.” *Bulletin of the Seismological Society of America* 84 (3): 935–53.

Linville, Lisa, Kristine Pankow, Debi Kilb, and Aaron Velasco. 2014. “Exploring Remote Earthquake Triggering Potential across EarthScopes’ Transportable Array through Frequency Domain Array Visualization.” *Journal of Geophysical Research: Solid Earth* 119 (12): 8950–63. https://doi.org/10.1002/2014JB011529.

McNamara, Daniel E., and Raymond P. Buland. 2004. “Ambient Noise Levels in the Continental United States.” *Bulletin of the Seismological Society of America* 94 (4): 1517–27. https://doi.org/10.1785/012003001.

Pankow, Kris L., Walter J. Arabasz, James C. Pechmann, and Susan J. Nava. 2004. “Triggered Seismicity in Utah from the 3 November 2002 Denali Fault Earthquake.” *Bulletin of the Seismological Society of America* 94 (6B): S332–47. https://doi.org/10.1785/0120040609.

Prejean, S. G., D. P. Hill, E. E. Brodsky, S. E. Hough, M. J. S. Johnston, S. D. Malone, D. H. Oppenheimer, A. M. Pitt, and K. B. Richards-Dinger. 2004. “Remotely Triggered Seismicity on the United States West Coast Following the Mw 7.9 Denali Fault Earthquake.” *Bulletin of the Seismological Society of America* 94 (6B): S348–59. https://doi.org/10.1785/0120040610.

“Quality and Completeness of UUSS Catalog Data: 1981-Present | U of U Seismograph Stations.” n.d. Accessed May 8, 2019. https://quake.utah.edu/regional-info/earthquake-catalogs/catalog-details/quality-and-completeness-of-uuss-catalog-data-1981-present.

Smith, Robert B., and Marc L. Sbar. 1974. “Contemporary Tectonics and Seismicity of the Western United States with Emphasis on the Intermountain Seismic Belt.” *GSA Bulletin* 85 (8): 1205–18. https://doi.org/10.1130/0016-7606(1974)85<1205:CTASOT>2.0.CO;2.

Stein, Seth, and Mian Liu. 2009. “Long Aftershock Sequences within Continents and Implications for Earthquake Hazard Assessment.” *Nature* 462 (7269): 87–89. https://doi.org/10.1038/nature08502.

Valastro, S., E. Mott Davis, and Alejandra G. Varela. 1972. “University of Texas At Austin Radiocarbon Dates IX.” *Radiocarbon* 14 (2): 461–85. https://doi.org/10.1017/S0033822200059506.

Velasco, Aaron A., Richard Alfaro-Diaz, Debi Kilb, and Kristine L. Pankow. 2016. “A Time-Domain Detection Approach to Identify Small Earthquakes within the Continental United States Recorded by the USArray and Regional NetworksTime-Domain Detection Approach to Identify Small Earthquakes within the Continental U.S.” *Bulletin of the Seismological Society of America* 106 (2): 512–25. https://doi.org/10.1785/0120150156.

Velasco, Aaron A., Stephen Hernandez, Tom Parsons, and Kris Pankow. 2008. “Global Ubiquity of Dynamic Earthquake Triggering.” *Nature Geoscience* 1 (6): 375–79. https://doi.org/10.1038/ngeo204.

Warren-Smith, Emily, Bill Fry, Yoshihiro Kaneko, and Calum J. Chamberlain. 2018. “Foreshocks and Delayed Triggering of the 2016 MW7.1 Te Araroa Earthquake and Dynamic Reinvigoration of Its Aftershock Sequence by the MW7.8 Kaikōura Earthquake, New Zealand.” *Earth and Planetary Science Letters* 482 (January): 265–76. https://doi.org/10.1016/j.epsl.2017.11.020.

Wei, Meng, Yoshihiro Kaneko, Pengcheng Shi, and Yajing Liu. 2018. “Numerical Modeling of Dynamically Triggered Shallow Slow Slip Events in New Zealand by the 2016 Mw 7.8

Kaikoura Earthquake." *Geophysical Research Letters* 45 (10): 4764–72. https://doi.org/10.1029/2018GL077879.

Vita

David Guenaga was born in San Bernardino, California. He graduated from Summit Leadership Academy High Desert High school and was given an Award of Excellence during his senior year. He also earned his Bachelor of Science degree in Geophysics from the University of California, Riverside in 2015 during which he received Academic Excellence Award. He joined UTEP's doctoral program in Geological Sciences in 2017. Mr. Guenaga is a recipient of the DGS/Karen Kellogg Shaw Memorial Scholarship and Earl D. and Reba C. Griffin Memorial Scholarships. He has also been selected to receive the Science, Mathematics, and Research for Transformation (SMART) scholarship provided by the National Defense Education Program. As part of the SMART scholarship, he will be interning at the Naval Oceanographic Office (NAVOCEANO) in Stennis Space Center, MS for the Department of Defense. Furthermore, upon graduation from his Ph.D., he will work for NAVOCEANO an additional two and a half years. Upon completion of his service, he will then be offered a permanent position with the Department of Defense.

Contact Information: dlguenaga@utep.edu (Alternative: davidguenaga@gmail.com)

This thesis/dissertation was typed by David Guenaga